CFD Letters www.cfdl.issres.net Vol. 3 (1) – March 2011

Experiments and numerical simulations on the aerodynamics of the Ahmed body

W. Meile[1], G. Brenn[1], A. Reppenhagen[2], B. Lechner[2], A. Fuchs[2C]

[1]*Institute of Fluid Mechanics and Heat Transfer (ISW), Graz University of Technology, Inffeldgasse 25/F, 8010 Graz, AUSTRIA*
[2]*The Virtual Vehicle Competence Center (ViF), Inffeldgasse 21a, 8010 Graz, AUSTRIA*

Received: 07/09/2010 – Revised 24/09/2010 – Accepted 27/09/2010

Abstract

The aerodynamic behaviour of the Ahmed body is investigated experimentally and numerically. The experiments cover the two slant angles 25° and 35° and Reynolds numbers up to $2.784 \cdot 10^6$. The commercial CFD tool Fluent™ v6.3.26 is tested for its ability to reproduce the aerodynamic force coefficients of the body. The simulations are validated with the present experiments and experiments from literature. Fair agreement with data from literature is found for velocity profiles along the slant and in the wake of the body.

Keywords: Ahmed body; vehicle aerodynamics; force measurement; comparison simulation/measurement results

1. Introduction

Optimized external car aerodynamics is necessary to achieve efficient vehicles with minimized fuel consumption, CO_2 emissions, and noise, while keeping a good driving stability. Steadily increasing computer power has been raising the importance of simulating the external aerodynamics of vehicles and computing the corresponding aerodynamic characteristic numbers. At present, an efficient resource management gains increased importance everywhere. A substantial part of the development time of cars is therefore invested in optimization. This is possible only and particularly by virtual development. In order to establish such development processes in the car industry, reliable simulation models validated by experiments are needed.

Model experiments suitable for providing validation data make use of model bodies with geometries characterized by variable parameters, such as the slant angle at the back. One such body is the Ahmed body, a bluff model body of simple shape with basic aerodynamic properties of a vehicle, which has been used for many reference investigations. The first measurements on the influence of the slant angle in the range between 0° and 40° at a flow velocity of 60 m/s (Re = $4.29 \cdot 10^6$) were carried out using a slightly different geometry, the so-called Morel body [1]. Ahmed et al. [2] carried out measurements with the same boundary conditions, using their nowadays so-called Ahmed body. Later, surface pressures and drag forces were measured at full scale Reynolds numbers by Bayraktar et al. [3]. Their model was 4.7 times larger than the original Ahmed body.

[C] Corresponding Author: Anton Fuchs
Email: anton.fuchs@v2c2.at, Tel: +43 316 873-9091, Fax: -9002
© 2009-2012 All rights reserved. ISSR Journals PII: S2180-1363(11)3132-X

Further measurements on pressure distribution, velocity, and turbulence properties of the flow around the Ahmed body were carried out by Lienhart et al. [4].

The aim of the present study is to investigate experimentally the aerodynamic behaviour of the Ahmed body under varying geometrical conditions and to test the ability of the CFD simulation package Fluent™ v6.3.26 to reproduce the experimental data. The simulations are validated using data acquired in the wind tunnel of the ISW and also compared with the results of [4].

Our paper is organised as follows: we first briefly introduce the experimental technique and the geometric and aerodynamic properties of the Ahmed body. In section 3 we introduce the methodology of the numerical simulations. Thereafter we present the results from experiments and simulations, including their comparison. The summary and conclusions are given in section 5.

2. Experimental technique and Ahmed body geometry

The geometrical shape of the Ahmed body investigated is depicted in Figure 1. Despite the considerable deviation of its geometry from usual vehicles, the body represents the basic aerodynamic properties of a vehicle, especially in the rear part. The slant angle φ has a strong influence on the aerodynamic drag and lift at the back. Both the drag and lift coefficients change abruptly at the angle φ=30°. Therefore, this angle is called the critical slant angle.

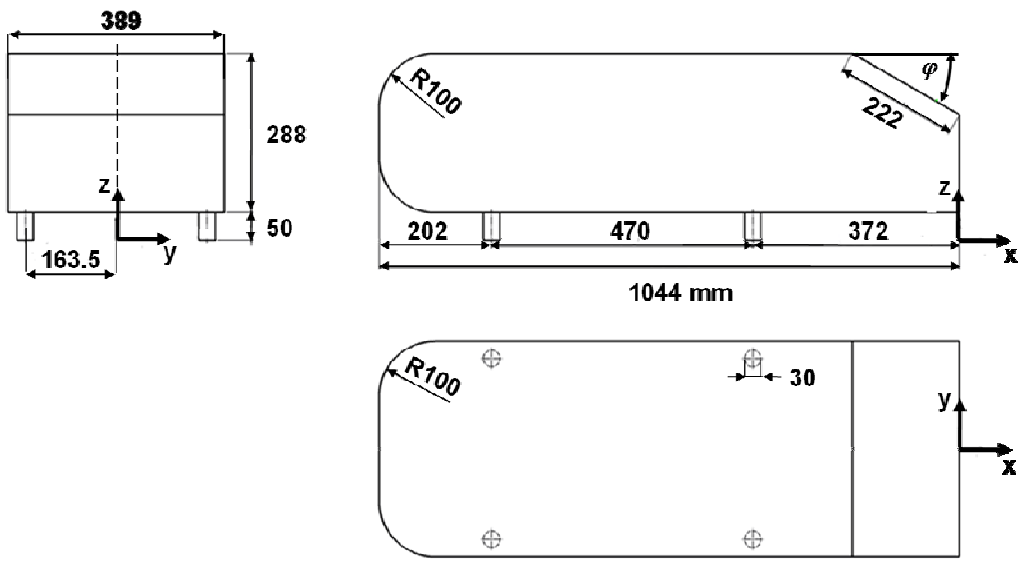

Figure 1: Geometry of the Ahmed body (adapted from [5])

We investigate the influence of the slant angle by measurements at φ = 25° and 35°. For slant angles φ ≤ 30°, an inward rotating pair of vortices with increasing strength is generated, as observed at fastback vehicles [6]. Therefore, the Ahmed body with the slant angle of 25° belongs to the fastback vehicles, which exhibit very strong inward rotating longitudinal vortices at the C-pillars. These vortices extend far into the wake and generate a field of downwind in the enclosed region. At a slant angle of 30°, i.e., directly before transition to the full squareback flow, this pair of vortices is developed most strongly, and the flow separates at the lower edge of the slant. This produces strong underpressures at that position, so that the aerodynamic drag reaches its maximum in this state [2].

The Ahmed body used for the measurements was built from wooden materials in the original dimensions shown in Figure 1. The rear part was interchangeable, so as to realise the two slant angles to be investigated with the same front part of the body.

The experimental part of the present investigations was performed in the 2 m low-speed aerodynamic wind tunnel of the ISW at Graz University of Technology. This wind tunnel is of the

Göttingen type with a ¾-open test section (2 m × 1.46 m) and closed return, and is designed for vehicle aerodynamics and general purpose applications. A detailed description is given in [7].

The forces and moments on the Ahmed body were measured at a velocity of 40 m/s for the two slant angles $\varphi = 25°$ and 35° for a yawing angle $\beta = 0°$. In order to determine the influence of the Reynolds number and to test for the existence of a hysteresis, the forces on the body were measured for the four air velocities 10, 20, 30, 40 m/s, each with increasing and with decreasing sense of the velocities. In order to achieve reliably steady mean values, three measurements were carried out for each air velocity, each for 15 s.

To enable a direct comparison with experimental data from the literature, the tare loads of the stilts were determined in separate measurements and subtracted from the full loads. In order to measure these tare loads, the model was held in place with a separate suspension, while the connection to the stilts was loosed. The cross sectional area of the model perpendicular to the longitudinal axis of the test section is $A = 0.112\ m^2$ and, therefore, the blockage ratio of the test section at $\beta = 0°$ is 3.8%.

3. Numerical simulations

Next to the experimental investigations, the flow around the Ahmed body in the wind tunnel was simulated with the commercial CFD tool Fluent™ v6.3.26. The Reynolds stress turbulence model was applied to account for the turbulent nature of the flow, with the non-equilibrium wall function method for near-wall treatment. The discretisation was 2nd order for the pressure, and 2nd order upwind for the other variables [8-9]. The overall solution procedure is iterative and based on the SIMPLE algorithm [10], which ensures a coupling between the velocity and pressure fields. A numerical wind tunnel was defined with dimensions according to the ERCOFTAC recommendations for test case 9.4 [11]. For a short and unique description of the individual test cases we applied strings of characters of the form ‘Aφβ’, where A represents the Ahmed body, φ the slant angle, and β the yawing angle. The string ‘A250’, for example, denotes an experiment with $\varphi = 25°$ and $\beta = 0°$.

In view of the computational costs, we had to seek for a suitable compromise in terms of grid resolution. The grids were chosen as coarse as possible to keep the computational effort within limits, and as fine as possible to resolve important flow phenomena. The grids were generated with the meshing tool SPIDER™ developed by Kickinger [12]. Regions of the flow field, where significant changes are expected, such as, e.g., the wake of the model, were refined separately. Depending on the slant angle φ, hex-dominant hybrid meshes with 4.5 to 5 million cells were generated. A sketch of the computational domain in the configuration ‘A250’ is depicted in Figure 2.

The entrance to the numerical wind tunnel is defined as a velocity-inlet boundary (see Figure 2). The condition is set as a uniform normal velocity of 40 m/s. At the wind tunnel exit, a pressure outlet boundary condition was set. The upstream region was chosen very long in order to avoid any feedback from the model to the inlet boundary. The correct no-slip condition would then yield a too thick boundary layer at the model location. For the ERCOFTAC test case 9.4, a boundary layer thickness of $\delta = 30$ mm at $x = -1.444$ m was specified. For this reason, i.e. to adjust the boundary layer thickness according to the recommended value, we applied a slip condition throughout the first part of the test section floor from $x = -6.5$ m to $x = -3.4$ m.

4. Results from experiments and simulations

In the following sections we first validate the experimental results from the present wind tunnel measurements by comparison with corresponding data from the literature. Then we compare the results from the simulations with the experimental data.

4.1 Comparison of experimental results from various sources: drag coefficient

Figure 3 displays the drag coefficient of the Ahmed body measured in the present study as a function of the Reynolds number for the slant angle φ = 25° and symmetrical flow (β = 0°). The measurements were carried out in the velocity range 10 m/s ≤ U_∞ ≤ 40 m/s. The maximum velocity corresponds to a Reynolds number of Re = $2.784 \cdot 10^6$. The data of Ahmed et al. [2] at Re = $4.29 \cdot 10^6$ are included for comparison. The data found by Bayraktar et al. [3] at full scale Reynolds numbers are quite similar to those of Ahmed et al. at the corresponding Reynolds number. The curve fit through the present data includes the values reported in [2] and [3] and so extends over one order of magnitude in the Reynolds number. This indicates that the present measurements reproduce the earlier reference data very accurately.

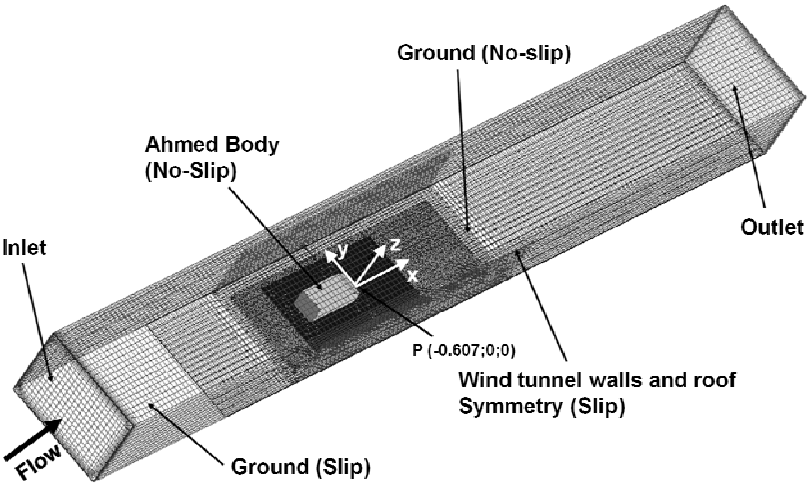

Figure 2: Computational domain with the configuration 'A250' (length/width/height = 15 m/1.87 m/1.4 m)

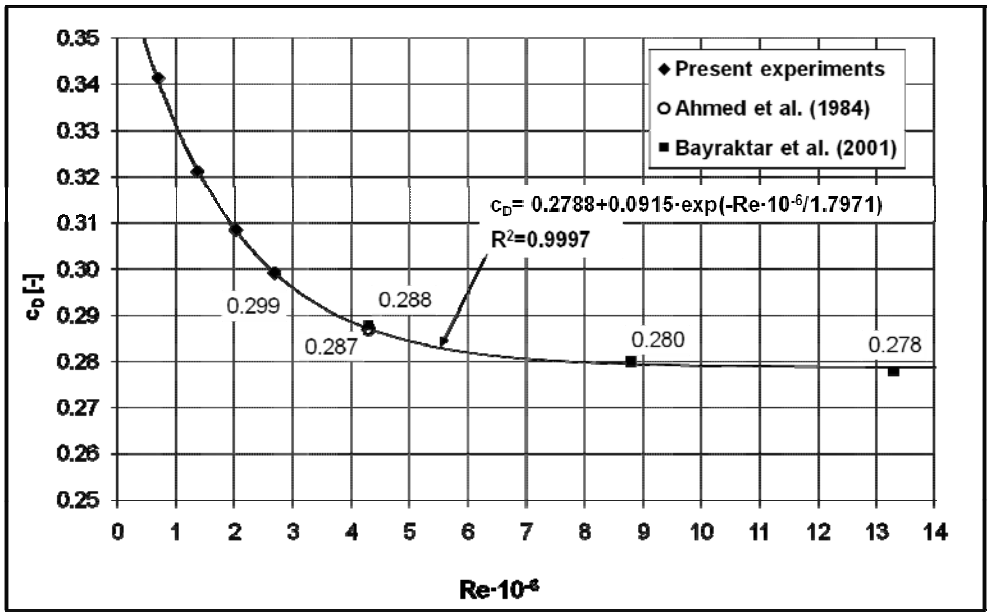

Figure 3: Drag coefficient vs. Reynolds number, φ = 25°

In the lower Reynolds number regime $0.7 \cdot 10^6 \leq Re \leq 2.7 \cdot 10^6$ covered by the present measurements, the drag coefficient varies by about 13%, while for larger Re this dependency is less pronounced. Bayraktar et al. [3] report a decrease of c_D by about 3.5% over the investigated range $4.29 \cdot 10^6 \leq Re \leq 13.2 \cdot 10^6$. Their data show the major part of the decrease up to $Re \approx 9 \cdot 10^6$, and a much less pronounced variation with the Re number above this threshold. This closely corresponds to the usually moderate Reynolds number dependence of the drag coefficient of modern passenger cars in the range $0.26 \leq c_D \leq 0.50$, as reported in [6].

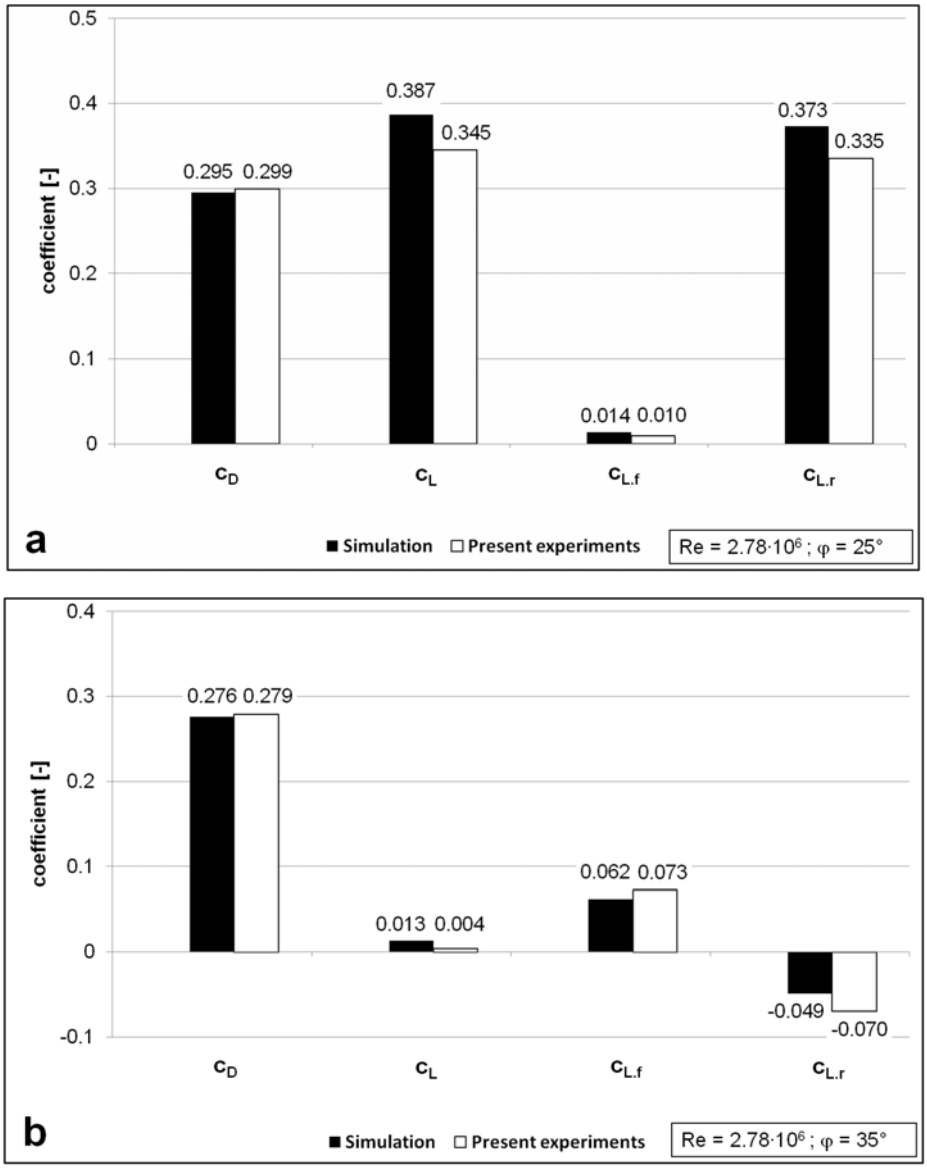

Figure 4. Drag (c_D) -, lift (c_L) -, lift front-axle ($c_{L.f}$)-, lift rear-axle ($c_{L.r}$) - coefficients of the Ahmed body for the slant angles (a): $\varphi = 25°$ and (b): $\varphi = 35°$; both (a) and (b) for $\beta = 0°$ and $y = 0$

Figure 4 shows that the numerical results agree well with our measurement results for symmetrical flow ($\beta = 0°$). Especially the drag is well predicted. In the case of $\varphi = 25°$ the forces are over-predicted with varying deviation (e.g. 42 lift points or about 12% for the lift coefficient c_L). For the larger slant angle $\varphi = 35°$, the forces are mainly under-predicted (especially the rear axle lift, while the front axle lift is fairly captured).

Due to the substantial impact of the slant angle on the flow behaviour, a further focus will be on the flow over the rear part of the model, and especially on the near wake region. Here we concentrate again on symmetrical flow at $\beta = 0°$ over the Ahmed body with the two slant angles 25° and 35°. Further comprehensive data sets are available for these cases, such as, e.g., pressure profiles and LDA data of the velocity distribution in the symmetry plane along the slant and in the wake [11].

4.2 Velocity profiles along the slant and in the wake

The following diagrams depict the streamwise velocity profiles at various x positions in the symmetry plane (y = 0) along the Ahmed body and in the wake for both slant angles φ = 25° and 35°. The profiles in corresponding diagrams are plotted in the same scale with the origin and the axis labelling omitted, as usual. The experimental data from the ERCOFTAC database were measured by Lienhart et al. [4]. The corresponding coordinate system is depicted in Figure 1.

The profiles along the body with φ = 25° and in the wake are depicted in Figure 5a. The data in Figure 5a correspond to the coordinates x = -262; -212; -162; -112; -62; -12; 38; 88; 138; 188; 238; 288; 338 (all values in mm).

The corresponding velocity profiles for the larger slant angle φ = 35° are displayed in Figure 5b. The profiles in Figure 5b correspond to the coordinates x = -263; -213; -163; -113; -63; -13; 37; 87; 137; 187; 237; 287; 337 (all values in mm).

From Figure 5a we see that the experimental data along the slant are well reproduced by the simulation. Even in the wake, the results of the simulation agree quite well with the experiments, with only minor deviations. The good agreement of the data for the flow between the wind tunnel floor and the under body of the model meets the expectations.

Although the velocity profiles from the simulation compare well with the experimental data some differences are obvious. Therefore, it is promising that the simulation results especially for the drag forces match the experimental data so well for both slant angles.

5. Summary, conclusions, and outlook

In the present study, the aerodynamic behaviour of the Ahmed body with two different rear slant angles was investigated by wind tunnel experiments and numerical simulations. Since many experimental data in the literature were acquired at different Reynolds numbers, one part of the study was focused on wind tunnel experiments to provide reliable data on forces and moments at the same Reynolds number. One major goal was to acquire the basis for the validation of results from CFD simulations on vehicle aerodynamics, which gain ever more interest in industrial development processes. The present wind tunnel measurements compare well with data from the literature at zero yawing angle.

Numerical simulations with the commercial CFD software package FLUENT™ v6.3.26 employ the Reynolds Stress Model (RSM) of turbulence, combined with the non-equilibrium wall function method for near-wall treatment. The simulation results are in good agreement with the measurements for symmetrical flow in both cases of the slant angle, especially for the drag. Although absolute values from measurements could not be fully matched, the trends of the changes were predicted well. The computed velocity profiles compare fairly well with the measurements of Lienhart et al. [4] for both slant angles, along the slant as well as in the wake. The good reproduction of velocity and pressure distributions around the body is the reason for the good match of the force coefficients found in our simulations. We may conclude that simulations with a spatial grid resolution and turbulence modelling as presently employed are a valuable tool for the design process in the car industry, even at the early stage, since the results achieved are indicative and the

simulations may be carried out in a reasonably short time. An improvement of the simulations may be achieved by even finer resolution of the computational grid in regions of the flow field with high gradients of the flow variables, plus a refined turbulence modelling.

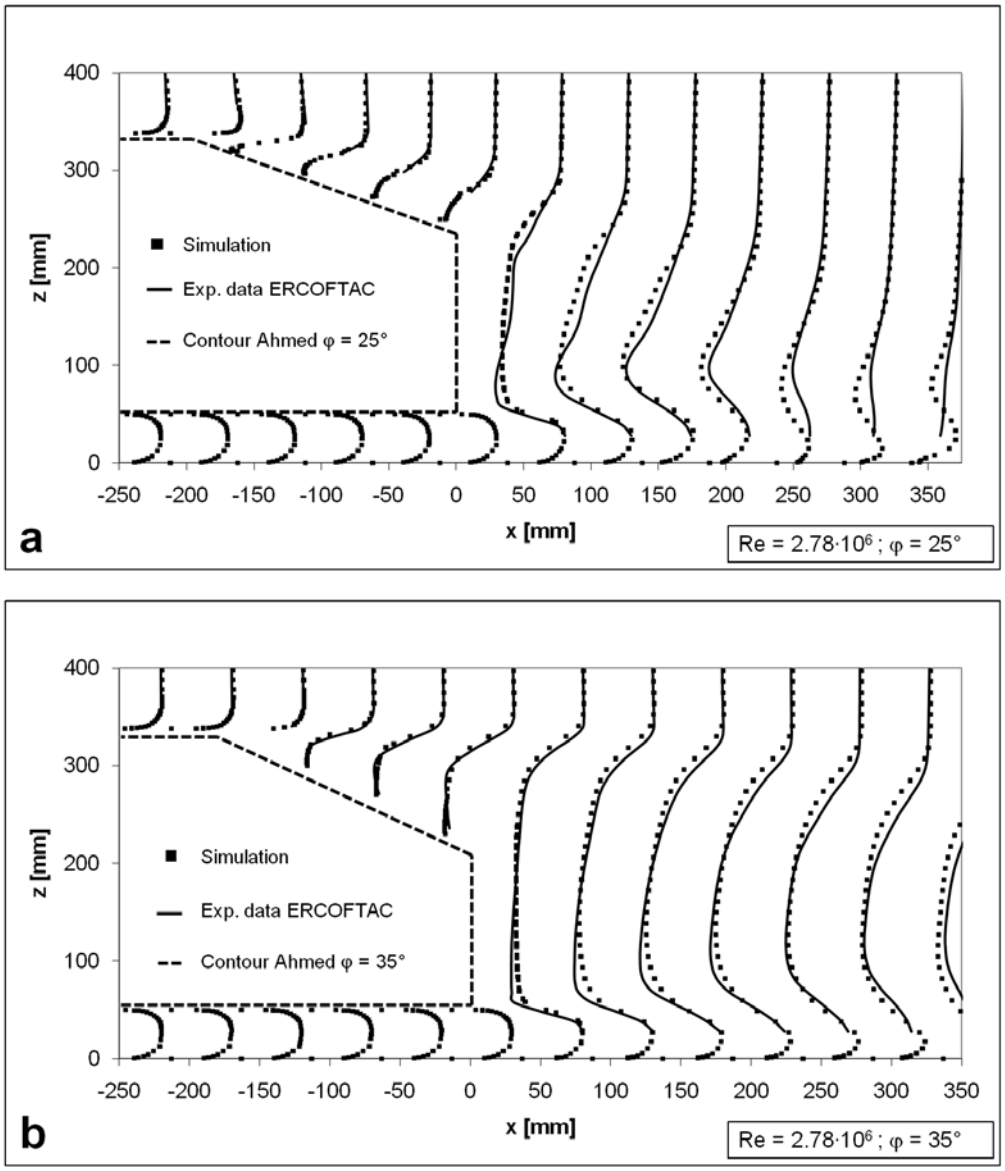

Figure 5: Profiles of the streamwise velocity component along the rear part of the Ahmed body for the slant angles (a): $\varphi = 25°$ and (b): $\varphi = 35°$; both (a) and (b) for $\beta = 0°$, $y = 0$

ACKNOWLEDGEMENTS

The authors gratefully acknowledge financial support from: “K2 Kompetenzzentren-Programm” of the Austrian Federal Ministry of Transport, Innovation, and Technology (BMVIT), Österreichische Forschungsförderungsgesellschaft mbH (FFG), Das Land Steiermark, and the Steirische Wirtschaftsförderung (SFG). Furthermore, the support of this project by the industrial partner MAGNA STEYR Fahrzeugtechnik AG & Co KG (Graz) is gratefully acknowledged. Many thanks go to the software provider ANSYS Germany GmbH for their support.

References

[1] Morel, T. (1978) The effect of base slant on the flow pattern and drag of three-dimensional bodies with blunt ends, In: Sovran G, Morel T, Mason WT (Eds.) Aerodynamic drag mechanisms of bluff bodies and road vehicles. Plenum Press, New York, 191-226.

[2] Ahmed, S.R., G. Ramm, G. Faltin (1984) Some salient features of the time-averaged ground vehicle wake, SAE paper 840300.

[3] Bayraktar, I., D. Landman, O. Baysal (2001) Experimental and computational investigation of Ahmed body for ground vehicle aerodynamics, SAE paper 2001-01-2742.

[4] Lienhart, H., C. Stoots, S. Becker (2000) Flow and turbulence structures in the wake of a simplified car model (Ahmed model), DGLR Fach Symp. der AG STAB, Universität Stuttgart, November 15–17.

[5] Hinterberger, C., M. García-Villalba, W. Rodi (2004) Large eddy simulation of flow around the Ahmed body. In: McCallen R, Browand F, Ross J (Eds.) Lecture notes in applied and computational mechanics / The aerodynamics of heavy vehicles: trucks, busses, and trains, Springer Verlag.

[6] Hucho, W.H. (1994) Aerodynamik des Automobils, 3. Auflage, VDI – Verlag Düsseldorf.

[7] Gretler, W., W. Meile (1993) Der 2m-Windkanal am Institut für Strömungslehre und Gasdynamik der Technischen Universität Graz. ÖIAZ 138/3: 90-96.

[8] Launder, B.E., G.J. Reece, W. Rodi (1975) Progress in the development of a Reynolds-stress turbulence closure. J Fluid Mech 68(3):537 - 566.

[9] Barth, T.J., D.C. Jepersen (1989) The Design and Application of Upwind Schemes on unstructured Meshes. AIAA-89-0366 27th Aerospace Sciences Meeting January 9-12, 1989/Reno, Nevada

[10] Patankar, S.V., D.B. Spalding (1972) A calculation procedure for heat, mass and momentum transfer in three-dimensional parabolic flows, Int J Heat Mass Transfer 15: 1787-1806.

[11] ERCOFTAC - European Research Community on Flow, Turbulence and Combustion (2001, 2002). http://tmdb.ws.tn.tudelft.nl/workshop9/workshop01.html
http://tmdb.ws.tn.tudelft.nl/workshop10/case9.4/case9.4.html
http://www.ercoftac.org/fileadmin/user_upload/bigfiles/sig15/database/index.html

[12] Kickinger, F. (2005) Parallel mesh generation for large scale applications using hex-dominant meshes. In: Hülsemann F, Kowarschik M, Rüde U (Eds.) Frontiers in Simulation - 18th Symposium Simulationstechnique ASIM 2005 Proceedings, SCS Publishing House: 133-138.